ADVANCED ELECTRONIC MATERIALS
www.advelectronicmat.de

Air and Water-Stable n-Type Doping and Encapsulation of Flexible MoS_2 Devices with SU8

Yen-Cheng Kung, Nahid Hosseini, Dumitru Dumcenco, Georg E. Fantner, and Andras Kis**

Favorable mechanical and electrical properties motivate the use of 2D semiconductors in flexible electronic devices. One of the main challenges here is the absence of a practical doping strategy which should provide air-stable, tunable doping levels in a process with a low thermal budget. Here, it is shown that SU8, an epoxy-based photoresist, can be used for nondegenerate n-type doping of monolayer MoS_2. The doping level can be finely tuned via low-temperature annealing. The doping method exhibits good ambient stability. The high degree of mechanical flexibility and low processing temperature also allows the integration of SU8 coating with flexible MoS_2 FETs, where it can provide both controllable doping and act as an encapsulation layer. The demonstrated stability of the devices to bending and exposure to water confirms the attractiveness of using SU8 in flexible electronic devices based on 2D semiconductors in a simple, versatile and scalable approach.

Layered transition metal dichalcogenides (TMDCs) are receiving resurgent interest due to their interesting physical and chemical properties.[1] Their potential applications cover a wide range, including electronics,[2] optoelectronics,[3,4] nanoelectromechanical systems (NEMS),[5] spin-valleytronics,[6] and catalysis.[7] MoS_2 is the most widely studied semiconducting TMDC, in part due to its high stability. Its semiconducting nature and ultrathin body allow the realization of field-effect transistors with a large on–off ratio[2] while the atomic scale thickness can suppress short-channel effects at aggressively scaled gate lengths.[8,9] Favorable mechanical properties, with a high fracture strain of at least 10%[10] make MoS_2 and other 2D semiconductors good candidates for applications in flexible electronic devices and circuits.[11]

However, several technical challenges need to be overcome before flexible devices based on 2D materials become widely available. Among them, a stable and controllable doping method that is compatible with flexible substrates and low processing temperatures should be developed. Strategies based on exposure to plasma, intercalation, and implantation were only demonstrated on multilayer MoS_2[12–14] which is less interesting for optoelectronic applications due to its indirect bandgap. Substitutional doping with, for example, rhenium or niobium during CVD growth result in doping levels that cannot be modified after growth and are difficult to implement locally and selectively.[15,16] Chemical doping on the other hand, can be easily implemented due to the large surface to volume ratio of 2D materials.[17] Various molecular surface doping methods based on wet chemical treatment have been widely explored, but most of them are not air-stable and are difficult to control.[18–21] While doping strategies based on functionalizing 2D materials with noble metal nanoparticles offer air stability, they do not result in good uniformity.[22,23] Stable and controllable doping could be achieved using Cs_2CO_3 thin films by varying the film thickness[24] or phosphorus silicate glass (PSG) substrates through thermal and optical activation;[25] however, brittle Cs_2CO_3 films and PSG substrates are not suitable for flexible electronics. So far, a practical technique for achieving air-stable and controllable doping of MoS_2 using materials and processes that are compatible with flexible electronics is missing.

An effective encapsulation layer with good gas barrier performance is another key enabler for flexible devices based on MoS_2 and other 2D semiconductors. It is well known that the performance of MoS_2 FETs degrades in air due to surface adsorption of O_2 and H_2O.[26–28] Al_2O_3, HfO_2, and other high-κ inorganic dielectrics have been commonly used as encapsulation layers for layered 2D devices.[2,29] However, their brittleness makes them undesirable for applications in flexible electronics, where the encapsulation layer usually experiences the highest strain under bending. Hexagonal boron nitride, a layered insulating material, is a promising candidate for encapsulation of other 2D materials due to the clean and smooth interface free of dangling bonds, but encapsulation is performed using a material transfer process which has so far been restricted to laboratory scale.[30–32]

Dr. Y.-C. Kung, Dr. D. Dumcenco,[+] Prof. A. Kis
Electrical Engineering Institute
École Polytechnique Fédérale de Lausanne (EPFL)
CH-1015, Lausanne, Switzerland
E-mail: andras.kis@epfl.ch

Dr. Y.-C. Kung, Dr. D. Dumcenco, Prof. A. Kis
Institute of Materials Science and Engineering
École Polytechnique Fédérale de Lausanne (EPFL)
CH-1015, Lausanne, Switzerland

N. Hosseini, Prof. G. E. Fantner
Institute of Bioengineering
École Polytechnique Fédérale de Lausanne (EPFL)
CH-1015, Lausanne, Switzerland
E-mail: georg.fantner@epfl.ch

The ORCID identification number(s) for the author(s) of this article can be found under https://doi.org/10.1002/aelm.201800492.

[+]Present address: Department of Quantum Matter Physics, Université de Genève, CH-1211 Geneva, Switzerland

DOI: 10.1002/aelm.201800492

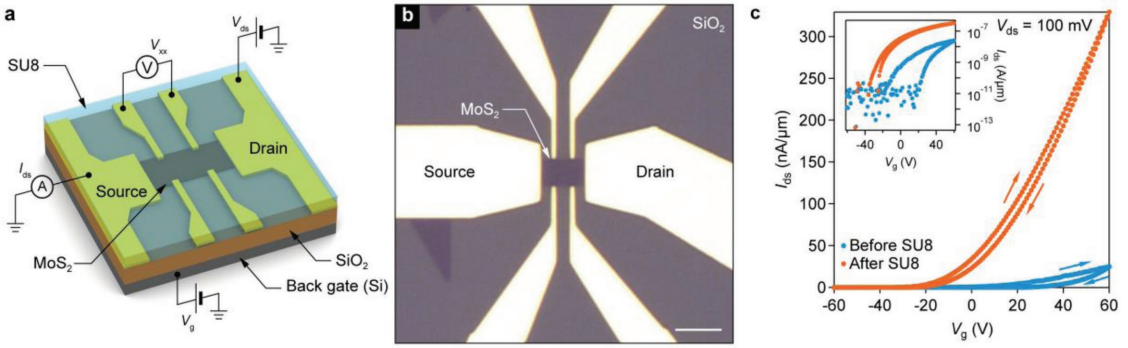

Figure 1. Bottom-gated monolayer MoS_2 FET with SU8 coating. a) Schematic of the device with an SU8 overlayer. b) Optical image of the device before applying SU8, scale bar is 5 μm. c) Transfer characteristic of the same MoS_2 FET before and after SU8 deposition. Inset: logarithmic scale plot of the transfer characteristic.

We propose using SU8 as a solution to these issues. Here, we demonstrate that SU8 can provide air-stable and controllable doping while at the same time acting as a gas and water barrier encapsulation layer, just like in the case of CNT and graphene devices.[33,34] Its mechanical flexibility and low processing temperature also make it compatible with flexible electronics. We show that the doping level can be easily tuned by simply extending the polymer baking time. We also fabricate flexible MoS_2 transistors that can be submerged in water for extended periods of time thanks to the protective SU8 coating while also being able to withstand bending to over 100 cycles of mechanical deformation.

We first evaluate the doping effect of SU8 on MoS_2 using bottom-gated field effect transistors fabricated on SiO_2/p^{++} Si substrates, **Figure 1**a,b. All our devices are based on CVD-grown monolayer MoS_2, in order to demonstrate the relevance of the SU8-based approach for large-area, scalable MoS_2. Devices were characterized before and after SU8 coating followed by a soft-bake process, with the transfer characteristic shown on Figure 1c. We find a large increase in on-current and a negative shift of the threshold voltage which is the result of n-type doping. The extracted carrier concentration of the doped MoS_2 is 2.4×10^{12} cm^{-2}, which is at a nondegenerate doping level as reflected by the preserved off-state current, Figure 1c inset. Previous reports of chemical doping of MoS_2 cover a wide range of doping levels, from $\approx 10^{10}$ to $\approx 10^{13}$ cm^{-2}, with a large variation resulting not only from different doping strategies but also intrinsic MoS_2 properties, the flake thickness and the interface charge state densities.[20,25,35,36]

The increased carrier concentration resulting from the n-type doping by SU8 reduces both the sheet resistance (R_s) and the Schottky barrier height between the metal contact. Since the contact resistance depends on these two quantities,[37] their reduction results in a smaller contact resistance R_c. Measurements on four-terminal devices (**Figure 2**a,b), show that both R_s and R_c are reduced by more than one order of magnitude after SU8 doping.

The SU8 solution contains SU8 epoxy, photo acid generator, and solvent (γ-Butyrolactone). Treating MoS_2 FET with only the solvent does not result in observable doping. On the other hand, treating another MoS_2 FET with the mixture of SU8 epoxy and the solvent, resulted in n-type doping, indicating that the SU8 epoxy is the main component of the SU8 solution responsible for the doping effect.

Raman spectroscopy was performed to observe the effect of SU8 on MoS_2. We have carried out measurements before and after SU8 coating on the same monolayer CVD-MoS_2 single crystal transferred onto a SiO_2/Si substrate. Raman-active A_{1g} and E_{2g} modes are commonly used as indicators of MoS_2 thickness and carrier concentration.[38,39] The Raman spectrum showing A_{1g} and E_{2g} modes of monolayer MoS_2 before and after SU8 coating is presented in Figure 2c. The Raman shift difference between A_{1g} and E_{2g} peaks is 18.65 cm^{-1} for our monolayer MoS_2 flake, which matches the reported value for monolayer MoS_2 in the literature.[38] After SU8 doping, the position of the E_{2g} peak does not change and the position of the A_{1g} peak shifts from 404 to 402.8 cm^{-1}. The linewidth of the E_{2g} peak does not change while the linewidth of the A_{1g} peak increases from 5.5 to 6.81 cm^{-1}. The softening and broadening of the A_{1g} peak are the signatures of n-type doping of MoS_2 flakes, consistent with a previous report on the effect of electrostatic doping[39] on the Raman spectrum of MoS_2, further confirming that SU8 induced n-type doping.

Controllable doping methods are essential for practical applications. Various strategies for tuning the doping levels within different ranges of doping have been reported in the literature. For methods based on wet chemistry, typical ways of tuning the doping level are based on controlling the exposure time to the doping agent and using solvents to remove the physisorbed molecules gradually. For example, Kiriya et al. reduced the doping from degenerate to nondegenerate levels by using toluene to remove benzyl viologen molecules, a process which required two days of immersion in toluene in order to realize the full tuning range.[35] Doping resulting from exposure to $(2\text{-Fc-DMBI})_2$, potassium, 1,2 dichloroethane, p-toluene sulfonic acid, and hydrazine have been tuned by altering the exposure time in the range from seconds to hours.[36,20,40,41] Apart from doping that involves wet chemistry, increasing the thickness of Cs_2CO_3 capping layers was also found to result in the monotonic increase of the doping level in the MoS_2.[24] Thermal and optical activation of PSG doping on MoS_2 provides a wide range of doping level modulation between 3.6×10^{10} and 8.3×10^{12} cm^{-2}, but the process requires high-temperature treatment at up to 900 °C.[25] Here, we provide a suitable solution for controllable doping on flexible MoS_2 devices, by taking into consideration that the ideal process should involve low temperatures while preserving mechanical flexibility and air

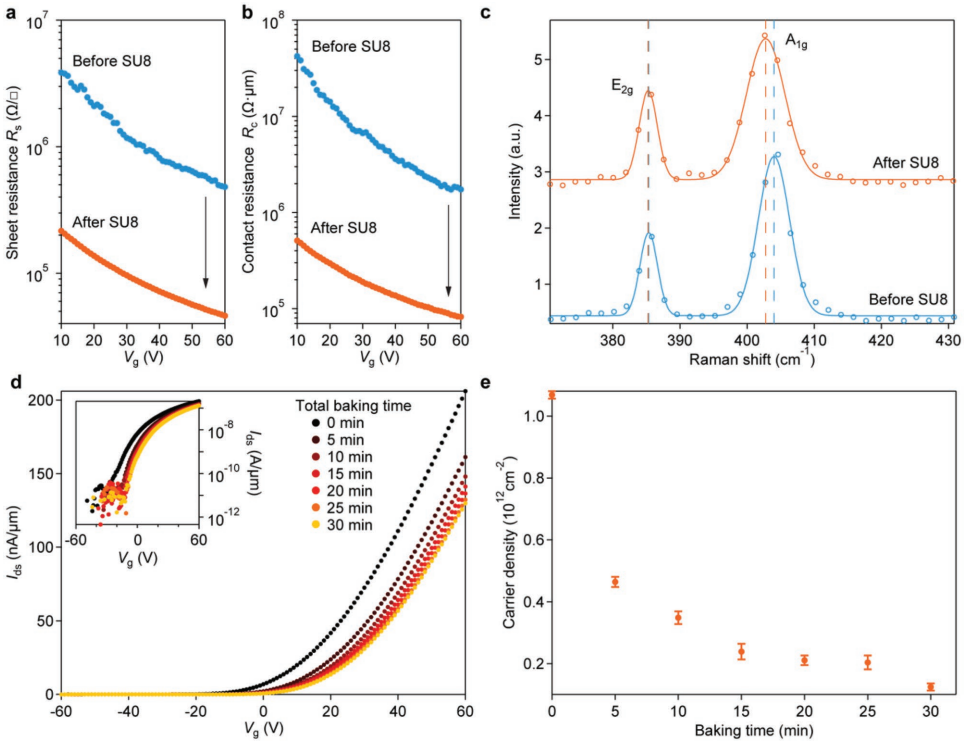

Figure 2. Effect of tunable SU8 doping on monolayer CVD-MoS_2. a,b) Sheet resistance and contact resistance of the same MoS_2 FET before and after SU8 doping. c) Raman spectrum of A_{1g} and E_{2g} peaks of a CVD-MoS_2 single crystal before and after SU8 doping. d) Transfer characteristic of an MoS_2 FET with SU8 doping. The device was annealed at 330 K with different baking times. Inset: log–lin plot of the transfer characteristic. e) Tuning carrier concentration of the SU8-doped MoS_2 with baking time. The carrier concentration decreases monotonically with increasing baking time.

stability. With SU8 treatment, the doping level of MoS_2 can be tuned by low-temperature annealing which does not damage the plastic substrates. We demonstrate the ability to tune the doping level by comparing device characteristics before and after the annealing treatment performed at 330 K for 5 min on SU8-coated MoS_2 FETs. This annealing treatment was repeated up to a total baking time of 30 min and all the measurements were performed at room temperature, Figure 2d. The transfer characteristic of the device shifts toward positive V_g with increasing baking time, reflecting decreasing electron concentration. The corresponding n-type doping level decreases monotonously from 1.07×10^{12} to 1.24×10^{11} cm^{-2}, Figure 2e. Details of the extraction of carrier concentration are described in Section S1 of the Supporting Information. The tuning range can be further expanded by increasing the annealing time and changing the parameters for the initial SU8 deposition. Our strategy involves a low energy cost and high production efficiency considering the low-temperature treatment and short annealing time used in the tuning process. Furthermore, compared to the chemical treatment methods, thermal activation generally results in a higher degree of process uniformity and simplicity.

Long-term stability of the doping level is a basic requirement for practical applications. Aging of the doping source itself and the influence of the environment due to O_2 and H_2O adsorbates[26–28] are the two main sources of instability. In our case, exposing uncoated monolayer MoS_2 FETs to air, results in a decrease of the on-current by a factor of more than 3 within 35 min of devices being removed from vacuum (Section S3, Supporting Information). On the other hand, SU8-coated devices demonstrate good gas barrier properties of SU8 by showing nearly no difference in device performance between air and vacuum (Figure S4, Supporting Information). Going further, we demonstrate longer-term air stability by exposing the device to air for 233 h and finding only minor changes in the transfer characteristic, as depicted in **Figure 3**a,b.

Encouraged by the favorable gas barrier properties, we further investigate water resistance of the SU8 layer. Bottom-gated flexible MoS_2 FETs on polyimide substrates were fabricated and coated with a 1 μm thick SU8 doping and encapsulation layer. The devices were kept in deionized water for over 65 h. The device performance was periodically measured after removing the sample from the water and drying it with N_2. As shown in Figure 3c, both the on and the off-state currents remained stable. Future work and optimization of SU8 deposition may result in an even better long-term stability while extending the study to saline-containing solutions could extend the field of applications to flexible electronic implants.

The high degree of mechanical flexibility and favorable electronic properties make MoS_2 and semiconducting TMDCs attractive materials for the realization of flexible FETs.[42,43] The low glass transition temperature of flexible polymer substrates used for the realization of such devices makes temperature a critical process parameter. SU8 is interesting in this context as a thermally tunable dopant with a relatively low processing temperature of less than 130 °C. There is an additional need

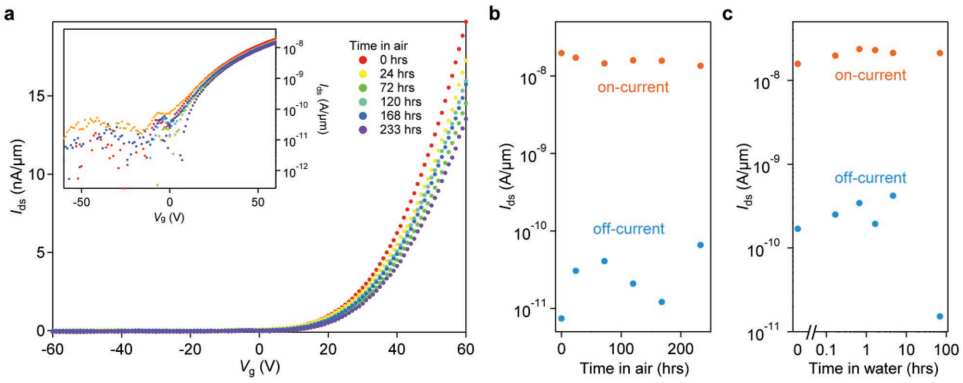

Figure 3. Stability of SU8-doped MoS_2 FETs. a) The evolution of the transfer characteristic for an SU8-doped MoS_2 FET kept in air over 9 days. b) The variation of on and off currents for the MoS_2 FET with SU8 doping over 9 days in air. c) The variation of on-current and off-current for a flexible MoS_2 FET with SU8 doping after submersion in deionized water for over 65 h. For each measurement, the device was removed from water and dried using an N_2 gun.

to develop a scalable encapsulation method for flexible MoS_2 transistors which could also solve the buckling issue observed in flexible MoS_2 devices under bending.[43] Our promising results on the stability of SU8-coated MoS_2 devices on rigid substrates motivate the integration of SU8 into flexible devices. The simplified process flow and the image of the device are shown in **Figure 4**a,b. The use of a 10 μm thick polyimide substrate together with a 1 μm SU8 encapsulation layer results in lightweight and easily bendable devices (Figure 4c). In Figure 4d,e, the consistent shift of the transfer characteristic curves toward negative gate voltages on multiple devices realized on the same chip reflects the good uniformity of the SU8-based doping method. The resilience of devices to bending was tested by applying strain along the direction of current flow through the channel. We first measure the devices in the flat state, and then bend them to a radius of 10 mm. We electrically characterize the device after releasing the strain and repeat the cycle 50 times. This is followed by an additional test run where we bend the device 50 more times to a radius of 7.5 mm. The uniaxial strain applied onto MoS_2 was estimated to be 0.048% and 0.064% for the bending radius of 10 and 7.5 mm respectively. Figure 4f,g shows the evolution of the transfer characteristic curve of the FET device undergoing the bending test. We observe a positive and saturating shift of the transfer characteristic curve over multiple bending cycles. The off current remains stable during the mechanical test, while the on-current showed a gradual decrease during the initial part of the test, reaching a stable level later on, Figure 4h. Overall, the devices show a stable on–off current ratio with changes of less than an order of magnitude over 100 bending cycles, similarly to other reports.[44–46]

The transfer characteristic of a device under strain is shown on Figure 4i. The measurement was performed after the multiple bending test in order to guarantee a stable and repeatable reference point for the relaxed state of the device. The data shown for the relaxed state are the average of the values before and after bending. The drain–source current is higher under a smaller bending radius, where a larger strain is applied to MoS_2. While expecting a 7% and 9% increase in current for a bending radius of 10 and 7.5 mm respectively from the piezoresistive effect in MoS_2,[47] we find a stronger increase of 49% and 63% at $V_g = 40$ V. This could be explained by different doping levels in our case and also a possible reduction in the contact resistance under strain.

In conclusion, we demonstrate n-type doping of monolayer CVD-MoS_2 induced by SU8 on monolayer CVD-MoS_2 with four-terminal electrical characterization and Raman spectroscopy. The doping level can be fine-tuned using low-temperature annealing at 330 K. Devices with SU8 encapsulation also show good air stability over a period of more than 9 days and good water resistance for more than 65 h. The low-temperature process and good barrier properties make SU8 an attractive material for encapsulating and doping flexible MoS_2 devices. We have also realized flexible MoS_2 FETs with SU8 encapsulation on 10 μm polyimide with devices showing only minor changes in performance after 100 cycles of bending. This study paves the way for the end-use of flexible MoS_2 FETs.

Experimental Section

Fabrication of Monolayer CVD-MoS_2 FETs on SiO_2/Si Substrates: Monolayer CVD-MoS_2 was grown on a *c*-plane sapphire substrate.[48] The film was transferred using PMMA A2 (MW = 950k, MicroChem) which was spin-coated on MoS_2/sapphire sample at 1500 rpm without baking. The coated sample was placed in a vacuum desiccator overnight to remove the solvent. The PMMA/MoS_2 film was released from the sapphire substrate by immersing the sample in 30%wt KOH at 75 °C for 30 min. The film was then rinsed using deionized water and picked-up with an SiO_2/Si substrate. The thickness of SiO_2 is 270 nm. After drying the sample on a hotplate at 75 °C, the sample was kept in acetone overnight to remove the PMMA. Annealing in furnace with gas flow of 100 sccm Ar and 10 sccm H_2 at 350 °C for 8 h was used to remove the PMMA residue. Electron beam lithography was used to pattern the metal contact and the etching mask. MMA EL6 (4000 rpm, 180 °C, 5 min) and PMMA A2 (1500 rpm, 180 °C, 5 min) double layer resist was used as an e-beam resist. An 85 nm thick Au layer acts as an electrode, covered with a 5 nm thick Ti layer on top in order to promote adhesion between SU8 and the electrical contacts. The contact stack is deposited by e-beam evaporation and the lift-off was performed in acetone. The sample was annealed for the second time in the furnace under a gas flow of 100 sccm Ar and 10 sccm H_2 at 250 °C for 8 h. MoS_2 channel was defined by O_2 plasma etching followed by acetone cleaning and device annealing with the same recipe to remove the resist residue and complete device fabrication. Electrical measurements are

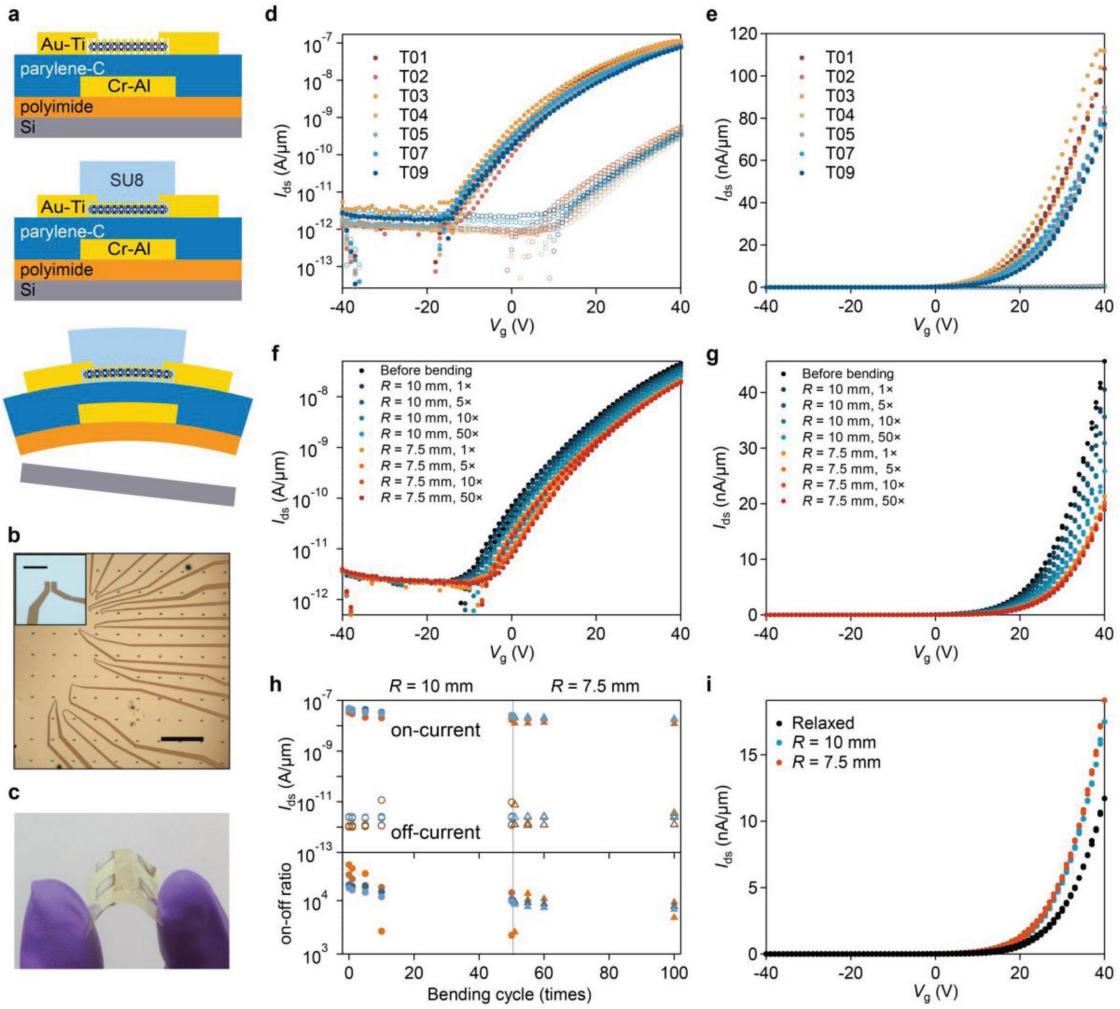

Figure 4. Flexible MoS_2 FETs on polyimide substrate with SU8 coating as the doping source and the encapsulation layer. a) The schematic and the simplified process flow for the fabrication of flexible MoS_2 FETs with an SU8 coating. b) Optical image of the device. The scale bar is 500 μm. Inset: optical image of a single device. The scale bar is 25 μm. c) Photograph of flexible devices under bending. d,e) Transfer characteristic for multiple flexible MoS_2 FETs before and after SU8 doping measured in air and shown on logarithmic and linear scales. The drain–source voltage is 100 mV. f,g) The evolution of the change of the transfer curve of a flexible MoS_2 FET over multiple bending cycles in log and linear scale. The device was first bent 50 times to a 10 mm bending radius, followed by bending to a 7.5 mm bending radius for 50 times. h) The change of on-current, off-current, and on–off ratio of four different devices, represented in different colors, over multiple bending cycles. i) The transfer characteristic curve of a device measured in the relaxed state and under bending. The measurement is performed after the bending test presented in parts (f) and (g).

then performed on these devices before and after SU8 treatment. For devices doped with SU8, the SU8 solution was drop-cast on top of the transistors, followed by soft baking in an oven. Samples were heated up with a ramp rate of 2 °C min^{-1} from 30 to 130 °C, maintained at 130 °C for 5 min and cooled-down with the same rate.

Fabrication of Flexible CVD-MoS2 FETs on Polyimide Substrate: 10 μm polyimide (PI2611, HD MicroSystems) was spin-coated on an Si wafer at 1200 rpm for 45 s with a ramp rate of 100 rpm s^{-1}. The sample was soft-baked on a hotplate at 120 °C and hard-baked in an oven with N_2 flow at 300 °C. Bottom gate (5 nm Cr and 50 nm Al) was deposited using an e-beam evaporator through shadow masks. A 200 nm thick parylene-C layer was deposited using chemical vapor deposition and used as the gate insulating layer. CVD-MoS_2 was transferred with the same method as mentioned above onto the parylene-C surface. The sample was immersed in acetone overnight and annealed in a furnace with a 200 sccm Ar flow at 200 °C for 4 h to remove the PMMA residue. Contact electrodes were formed using the same method as in the fabrication of devices on SiO_2/Si substrate mentioned above. SU8 layer 1 μm thick of (GM1040, Gersteltec sàrl) was spin-coated, followed by soft-bake, exposure, and postexposure bake. Finally, the polyimide substrate with fabricated devices on top was peeled-off from the silicon support manually.

Electrical Measurement of MoS_2 FETs: Electrical characterization was carried out using Agilent E5270B, National Instruments DAQ cards, SR570 current preamplifiers and SR560 low noise voltage preamplifiers.

Raman Spectrum Measurement of MoS_2 Flakes: Raman spectrum of CVD monolayer MoS_2 was measured using a Renishaw inVia Reflex Raman Confocal microscope with 532 nm laser source and grating of 1800 gr mm^{-1}.

Calculation of Neutral Plane and Strain of Flexible Devices: In a multilayer system, there are n layers where the bottom layer is the first layer. Then the distance γ between neutral plane and bottom surface of the first layer is given by $\gamma = \sum_{i=1}^{n} E_i t_i \left[\sum_{j=1}^{i} t_j - t_i/2\right] / \sum_{i=1}^{n} E_i t_i$.[49] E_i and t_i are the Young's moduli and the thickness of each layer. For the flexible MoS_2 FETs, the stack is composed of 10 μm polyimide, 5 nm Cr, 50 nm Al, 200 nm parylene-C, 0.7 nm MoS_2, and 1 μm SU8. The Young's moduli are $E_{polyimide}$ = 8.5GPa, E_{Cr} = 279 GPa, E_{Al} = 70 GPa, $E_{parylene}$ = 2.8 GPa,

$E_{MoS2} = 270$ GPa, and $E_{SU8} = 2.92$ GPa. The calculated y and the distance between MoS_2 and the neutral plane are 5.48 and 4.77 µm, respectively. The equation $\varepsilon = d/R$ was used to calculated the strain applied onto MoS_2 with ε the applied strain, R the bending radius, and d the distance between MoS_2 and the neutral plane of the sample.

Supporting Information

Supporting Information is available from the Wiley Online Library or from the author.

Acknowledgements

Y.-C. K. and N.H. contributed equally to this work. The authors thank Sébastien Jiquet for the discussion on SU8. Devices were fabricated in EPFL Center for Micro/Nanotechnology (CMI). The authors acknowledge the help of Z. Benes (CMI) with e-beam lithography. Y.-C.K., G.E.F., and A.K. acknowledge support from the Competence Centre for Materials Science and Technology Materials Challenge grant "Large Area Growth of 2D Materials for Device Integration." Y.-C.K. and A.K. would like to acknowledge support by the Marie Curie ITN network "MoWSeS" (Grant No. 317451) and the Swiss National Science Foundation (Grant No. 157739). A.K. acknowledges funding from the European Union's Horizon 2020 research and innovation programme under Grant Agreement Nos. 696656 and 785219 (Graphene Flagship Core 1 and Core 2). G.E.F. acknowledges funding from the European Union FP7/2007-2013/ERC under Grant Agreement No. 307338-NaMic and the European Union H2020 - Framework Programme for Research & Innovation (2014–2020); ERC-2017-CoG; InCell; Project number 773091.

Conflict of Interest

The authors declare no conflict of interest.

Keywords

2D transition metal dichalcogenides, doping, encapsulation, FET devices, flexible devices

Received: July 31, 2018
Revised: September 26, 2018
Published online:

[1] Q. H. Wang, K. Kalantar-Zadeh, A. Kis, J. N. Coleman, M. S. Strano, *Nat. Nanotechnol.* **2012**, *7*, 699.
[2] B. Radisavljevic, A. Radenovic, J. Brivio, V. Giacometti, A. Kis, *Nat. Nanotechnol.* **2011**, *6*, 147.
[3] O. Lopez-Sanchez, D. Lembke, M. Kayci, A. Radenovic, A. Kis, *Nat. Nanotechnol.* **2013**, *8*, 497.
[4] F. H. L. Koppens, T. Mueller, P. Avouris, A. C. Ferrari, M. S. Vitiello, M. Polini, *Nat. Nanotechnol.* **2014**, *9*, 780.
[5] A. Castellanos-Gomez, R. van Leeuwen, M. Buscema, H. S. J. van der Zant, G. A. Steele, W. J. Venstra, *Adv. Mater.* **2013**, *25*, 6719.
[6] D. Xiao, G.-B. Liu, W. Feng, X. Xu, W. Yao, *Phys. Rev. Lett.* **2012**, *108*, 196802.
[7] H. Li, C. Tsai, A. L. Koh, L. Cai, A. W. Contryman, A. H. Fragapane, J. Zhao, H. S. Han, H. C. Manoharan, F. Abild-Pedersen, J. K. Nørskov, X. Zheng, *Nat. Mater.* **2016**, *15*, 48.
[8] Y. Yoon, K. Ganapathi, S. Salahuddin, *Nano Lett.* **2011**, *11*, 3768.
[9] S. B. Desai, S. R. Madhvapathy, A. B. Sachid, J. P. Llinas, Q. Wang, G. H. Ahn, G. Pitner, M. J. Kim, J. Bokor, C. Hu, H.-S. P. Wong, A. Javey, *Science* **2016**, *354*, 99.
[10] S. Bertolazzi, J. Brivio, A. Kis, *ACS Nano* **2011**, *5*, 9703.
[11] D. Akinwande, N. Petrone, J. Hone, *Nat. Commun.* **2014**, *5*, 5678.
[12] S. Wi, H. Kim, M. Chen, H. Nam, L. J. Guo, E. Meyhofer, X. Liang, *ACS Nano* **2014**, *8*, 5270.
[13] J. Guo, F. Li, Y. Sun, X. Zhang, L. Tang, *J. Power Sources* **2015**, *291*, 195.
[14] A. Nipane, D. Karmakar, N. Kaushik, S. Karande, S. Lodha, *ACS Nano* **2016**, *10*, 2128.
[15] J. Suh, T.-E. Park, D.-Y. Lin, D. Fu, J. Park, H. J. Jung, Y. Chen, C. Ko, C. Jang, Y. Sun, R. Sinclair, J. Chang, S. Tongay, J. Wu, *Nano Lett.* **2014**, *14*, 6976.
[16] J. Gao, Y. D. Kim, L. Liang, J. C. Idrobo, P. Chow, J. Tan, B. Li, L. Li, B. G. Sumpter, T.-M. Lu, V. Meunier, J. Hone, N. Koratkar, *Adv. Mater.* **2016**, *28*, 9735.
[17] V. P. Pham, G. Y. Yeom, *Adv. Mater.* **2016**, *28*, 9024.
[18] Y. Li, C.-Y. Xu, P. Hu, L. Zhen, *ACS Nano* **2013**, *7*, 7795.
[19] Y. Du, H. Liu, A. T. Neal, M. Si, P. D. Ye, *IEEE Electron Device Lett.* **2013**, *34*, 1328.
[20] A. Tarasov, S. Zhang, M.-Y. Tsai, P. M. Campbell, S. Graham, S. Barlow, S. R. Marder, E. M. Vogel, *Adv. Mater.* **2015**, *27*, 1175.
[21] D.-H. Kang, M.-S. Kim, J. Shim, J. Jeon, H.-Y. Park, W.-S. Jung, H.-Y. Yu, C.-H. Pang, S. Lee, J.-H. Park, *Adv. Funct. Mater.* **2015**, *25*, 4219.
[22] D. Sarkar, X. Xie, J. Kang, H. Zhang, W. Liu, J. Navarrete, M. Moskovits, K. Banerjee, *Nano Lett.* **2015**, *15*, 2852.
[23] T. S. Sreeprasad, P. Nguyen, N. Kim, V. Berry, *Nano Lett.* **2013**, *13*, 4434.
[24] J. D. Lin, C. Han, F. Wang, R. Wang, D. Xiang, S. Qin, X.-A. Zhang, L. Wang, H. Zhang, A. T. S. Wee, W. Chen, *ACS Nano* **2014**, *8*, 5323.
[25] H.-Y. Park, M.-H. Lim, J. Jeon, G. Yoo, D.-H. Kang, S. K. Jang, M. H. Jeon, Y. Lee, J. H. Cho, G. Y. Yeom, W.-S. Jung, J. Lee, S. Park, S. Lee, J.-H. Park, *ACS Nano* **2015**, *9*, 2368.
[26] D. Jariwala, V. K. Sangwan, D. J. Late, J. E. Johns, V. P. Dravid, T. J. Marks, L. J. Lauhon, M. C. Hersam, *Appl. Phys. Lett.* **2013**, *102*, 173107.
[27] B. Baugher, H. O. H. Churchill, Y. Yang, P. Jarillo-Herrero, *Nano Lett.* **2013**, *13*, 4212.
[28] D. Lembke, A. Allain, A. Kis, *Nanoscale* **2015**, *7*, 6255.
[29] D. Kufer, G. Konstantatos, *Nano Lett.* **2015**, *15*, 7307.
[30] L. Wang, I. Meric, P. Y. Huang, Q. Gao, Y. Gao, H. Tran, T. Taniguchi, K. Watanabe, L. M. Campos, D. A. Muller, J. Guo, P. Kim, J. Hone, K. L. Shepard, C. R. Dean, *Science* **2013**, *342*, 614.
[31] A. Avsar, I. J. Vera-Marun, J. Y. Tan, K. Watanabe, T. Taniguchi, A. H. Castro Neto, B. Özyilmaz, *ACS Nano* **2015**, *9*, 4138.
[32] H. C. P. Movva, A. Rai, S. Kang, K. Kim, B. Fallahazad, T. Taniguchi, K. Watanabe, E. Tutuc, S. K. Banerjee, *ACS Nano* **2015**, *9*, 10402.
[33] H. Al-Mumen, L. Dong, W. Li, *Appl. Phys. Lett.* **2013**, *103*, 232113.
[34] H. Al-Mumen, *Micro Nano Lett.* **2015**, *10*, 670.
[35] D. Kiriya, M. Tosun, P. Zhao, J. S. Kang, A. Javey, *J. Am. Chem. Soc.* **2014**, *136*, 7853.
[36] H. Fang, M. Tosun, G. Seol, T. C. Chang, K. Takei, J. Guo, A. Javey, *Nano Lett.* **2013**, *13*, 1991.
[37] A. Allain, J. Kang, K. Banerjee, A. Kis, *Nat. Mater.* **2015**, *14*, 1195.
[38] C. Lee, H. Yan, L. E. Brus, T. F. Heinz, J. Hone, S. Ryu, *ACS Nano* **2010**, *4*, 2695.
[39] B. Chakraborty, A. Bera, D. V. S. Muthu, S. Bhowmick, U. V. Waghmare, A. K. Sood, *Phys. Rev. B* **2012**, *85*, 161403(R).
[40] S. Andleeb, A. Kumar Singh, J. Eom, *Sci. Technol. Adv. Mater.* **2015**, *16*, 035009.

[41] D. Lim, E. S. Kannan, I. Lee, S. Rathi, L. Li, Y. Lee, M. A. Khan, M. Kang, J. Park, G.-H. Kim, *Nanotechnology* **2016**, *27*, 225201.
[42] J. Pu, Y. Zhang, Y. Wada, J. T.-W. Wang, L.-J. Li, Y. Iwasa, T. Takenobu, *Appl. Phys. Lett.* **2013**, *103*, 023505.
[43] H.-Y. Chang, S. Yang, J. Lee, L. Tao, W.-S. Hwang, D. Jena, N. Lu, D. Akinwande, *ACS Nano* **2013**, *7*, 5446.
[44] J. Yoon, W. Park, G.-Y. Bae, Y. Kim, H. S. Jang, Y. Hyun, S. K. Lim, Y. H. Kahng, W.-K. Hong, B. H. Lee, H. C. Ko, *Small* **2013**, *9*, 3295.
[45] H.-Y. Chang, M. N. Yogeesh, R. Ghosh, A. Rai, A. Sanne, S. Yang, N. Lu, S. K. Banerjee, D. Akinwande, *Adv. Mater.* **2016**, *28*, 1818.
[46] M.-Y. Tsai, A. Tarasov, Z. R. Hesabi, H. Taghinejad, P. M. Campbell, C. A. Joiner, A. Adibi, E. M. Vogel, *ACS Appl. Mater. Interfaces* **2015**, *7*, 12850.
[47] S. Manzeli, A. Allain, A. Ghadimi, A. Kis, *Nano Lett.* **2015**, *15*, 5330.
[48] D. Dumcenco, D. Ovchinnikov, K. Marinov, P. Lazić, M. Gibertini, N. Marzari, O. L. Sanchez, Y.-C. Kung, D. Krasnozhon, M.-W. Chen, S. Bertolazzi, P. Gillet, A. Fontcuberta i Morral, A. Radenovic, A. Kis, *ACS Nano* **2015**, *4*, 4611.
[49] M. Kaltenbrunner, T. Sekitani, J. Reeder, T. Yokota, K. Kuribara, T. Tokuhara, M. Drack, R. Schwödiauer, I. Graz, S. Bauer-Gogonea, S. Bauer, T. Someya, *Nature* **2013**, *499*, 458.

ADVANCED ELECTRONIC MATERIALS

Supporting Information

for *Adv. Electron. Mater.,* DOI: 10.1002/aelm.201800492

Air and Water-Stable n-Type Doping and Encapsulation of Flexible MoS_2 Devices with SU8

Yen-Cheng Kung, Nahid Hosseini, Dumitru Dumcenco, Georg E. Fantner, and Andras Kis**

Supplementary Information for Air and water-stable n-type doping and encapsulation of MoS_2 flexible devices with SU8

Dr. Yen-Cheng Kung[1,2†], Nahid Hosseini[3†], Dr. Dumitru Dumcenco[1,2,‡], Prof. Dr. Georg Fantner[3*], Prof. Dr. Andras Kis[1,2*]

[1]Electrical Engineering Institute, École Polytechnique Fédérale de Lausanne (EPFL), CH-1015 Lausanne, Switzerland

[2]Institute of Materials Science and Engineering, École Polytechnique Fédérale de Lausanne (EPFL), CH-1015 Lausanne, Switzerland

[3]Institute of Bioengineering, École Polytechnique Fédérale de Lausanne (EPFL), CH-1015 Lausanne, Switzerland

[†]These authors contributed equally

[‡]Current address: Department of Quantum Matter Physics, Université de Genève, CH-1211, Geneva, Switzerland

*Correspondence should be addressed to: georg.fantner@epfl.ch and andras.kis@epfl.ch

1. Extraction of carrier concentration

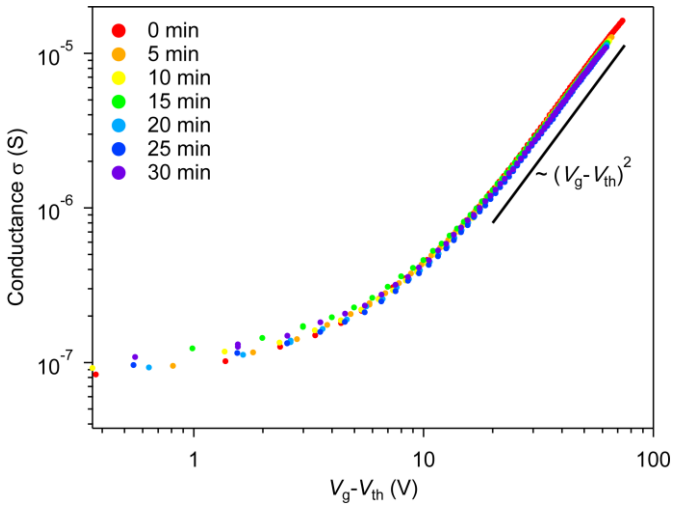

Figure S1. MoS_2 FET conductance σ extracted from 4-terminal measurements plotted as a function of $(V_g - V_{th})$ for different annealing periods showing a good fit to the expression $\sigma \sim (V_g - V_{th})^2$ at overdrive voltages above 20 V.

The extraction of carrier concentration N_{2D} at zero gate voltage is based on the expression $N_{2D} = C_{ox}(V_g - V_{th})/e$ where C_{ox} is the capacitance per unit area for the 270 nm thick SiO_2 and V_g is the gate bias voltage. V_{th} is the threshold voltage extracted from the intersect of $\sigma^{0.5}$ vs. V_g since $\sigma \sim (V_g - V_{th})^2$ when scattering from charged impurities is the dominant scattering mechanism.[1–3] At large carrier concentrations, charged impurities are screened and the conductance is proportional to the charge density n.[1–3]

2. The SU8 doping effect in vacuum and inert atmosphere

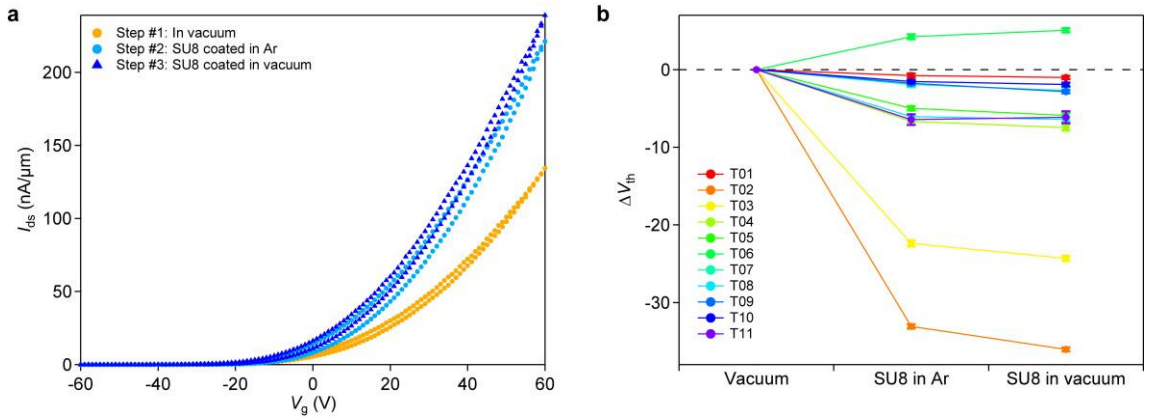

Figure S2. The SU8 doping effect under vacuum condition. **a**, Transfer characteristics of an MoS_2 FET measured in vacuum after vacuum annealing, in Ar environment after SU8 doping followed by measurement in vacuum. **b**, The change of the threshold voltage of multiple devices under different experimental conditions.

In order to remove the influence of water and oxygen adsorbates which could mask the doping effect of SU8, we have also performed the following experiment using two-terminal bottom-gated MoS_2 FETs. First, we characterize the device in vacuum (5×10^{-7} mbar) after annealing in vacuum at 140°C for 12 hours. The chamber is then sealed with a manual valve, disconnected and transferred into an Ar-filled glovebox. The device is removed from the chamber and doped using SU8. The device is kept in an Ar environment for the second measurement. The device is then transferred back into the vacuum chamber without exposing it to the atmosphere and a third measurement is performed in vacuum. Figure S2a shows a typical set of transfer characteristics for a device characterized in these three different conditions. We can clearly see the SU8 n-type doping effect by comparing the transfer characteristic curve before and after SU8 coating. On current increased and the threshold voltage shifted to negative voltages after SU8 doping. The same trend was observed in multiple devices as shown on Figure S2b where we plot the threshold voltage change ΔV_{th}. Ten out of eleven devices we tested showed a clear negative shift of threshold voltage after SU8 doping, indicating the n-type doping effect. The variation of the voltage shift could be caused by variations in the adhesion of SU8 on MoS_2.

3. Comparison of device performance with and without SU8 encapsulation

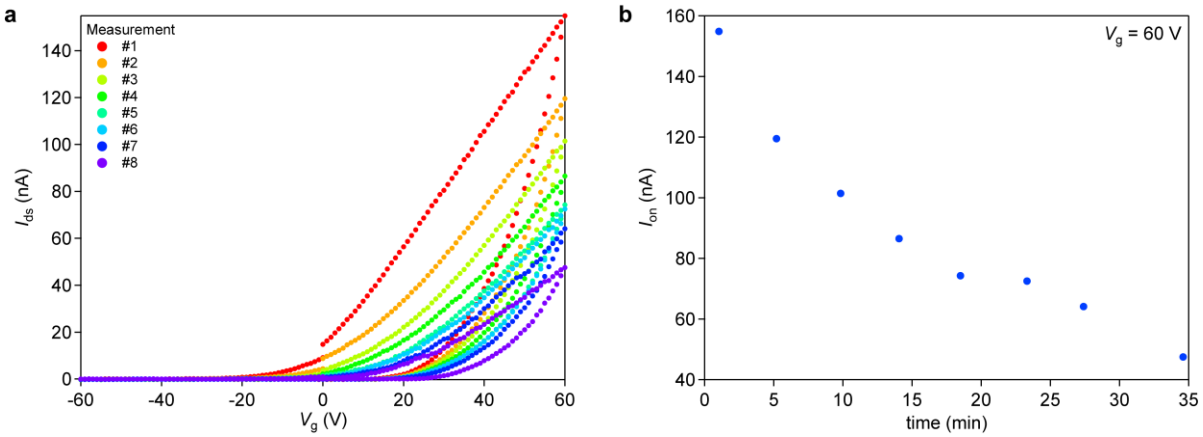

Figure S3. The performance degradation of a bottom-gated MoS_2 FET without SU8 encapsulation under ambient condition. **a**, Consecutively measured transfer characteristic curves of a MoS_2 FET right after exposure to air from vacuum. **b**, The evolution of the on-current recorded in air at V_g = 60 V.

The performance degradation of the device without encapsulation under ambient condition is shown in Figure S3. The gate voltage sweep started right after the device was exposed to air following annealing in vacuum. With each consecutive sweep, we can clearly see a drop in the current. Within 35 min, the on-current at a gate voltage V_g = 60 V decreased by more than a factor of 3 due to adsorption of atmospheric O_2 and H_2O on the MoS_2 surface.[4–6]

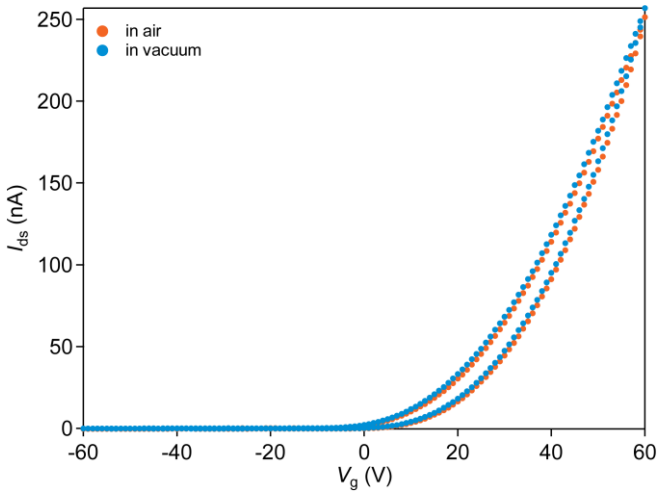

Figure S4. The transfer characteristic for an SU8-coated MoS_2 FET measured in air and under vacuum (1×10^{-6} mbar).

The MoS_2 FET coated with SU8 was measured in air and vacuum, and the transfer characteristics show negligible difference between the two conditions, proving that the SU8 layer can effectively block the influence of air on MoS_2.

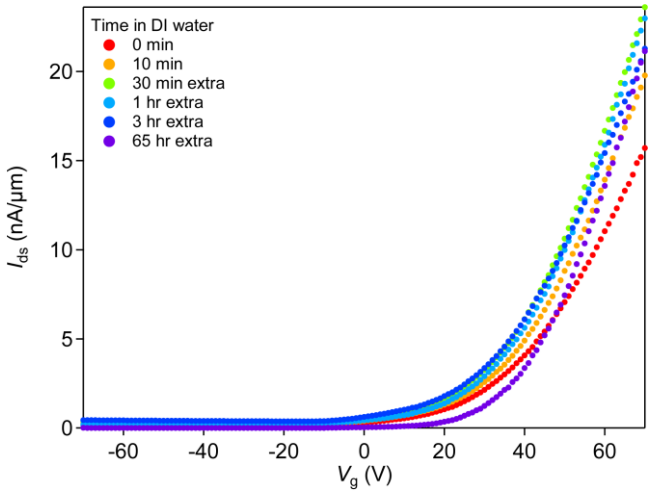

Figure S5. Water resistance of flexible MoS_2 FETs encapsulated with SU8. The figure shows the evolution of the transfer characteristics of the flexible device after having been submerged in water for a cumulative duration of over 65 hours. The device was taken out of the water and gently dried with N_2 gun before each measurement, after which it was returned to water.

REFERENCES

[1] S. Adam, S. Das Sarma, Phys. Rev. B **2008**, 77, DOI 10.1103/PhysRevB.77.115436.
[2] S. Ghatak, A. N. Pal, A. Ghosh, ACS Nano **2011**, 5, 7707.
[3] Y. Guo, X. Wei, J. Shu, B. Liu, J. Yin, C. Guan, Y. Han, S. Gao, Q. Chen, Appl. Phys. Lett. **2015**, 106, 103109.
[4] H. Qiu, L. Pan, Z. Yao, J. Li, Y. Shi, X. Wang, Appl. Phys. Lett. **2012**, 100, 123104.
[5] D. Jariwala, V. K. Sangwan, D. J. Late, J. E. Johns, V. P. Dravid, T. J. Marks, L. J. Lauhon, M. C. Hersam, Appl. Phys. Lett. **2013**, 102, 173107.
[6] D. Lembke, A. Allain, A. Kis, Nanoscale **2015**, 7, 6255.